European Journal of Mechanics B/Fluids 30 (2011) 89–98

Contents lists available at ScienceDirect

European Journal of Mechanics B/Fluids

journal homepage: www.elsevier.com/locate/ejmflu

Modelling the growth rate of a tracer gradient using stochastic differential equations

Lennon Ó Náraigh *

School of Mathematical Sciences, University College Dublin, Belfield, Dublin 4, Ireland

ARTICLE INFO

Article history:
Received 5 May 2010
Received in revised form
29 September 2010
Accepted 4 October 2010
Available online 15 October 2010

Keywords:
Turbulent mixing
Turbulence modelling
Fokker–Planck equation

ABSTRACT

We develop a model in two dimensions to characterise the growth rate of a tracer gradient mixed by a statistically homogeneous flow that varies on arbitrary timescales. The model is based on the orientation dynamics of the passive-tracer gradient with respect to the straining (compressive) direction of the flow, and involves reducing the dynamics to a set of stochastic differential equations. The statistical properties of the system emerge from solving the associated Fokker–Planck equation. Within the model framework, the tracer gradient aligns with the compressive direction when the mean effective rotation in the flow is zero. At finite values of rotation, the tracer gradient aligns with a different direction, but the mean growth rate of the gradient is positive in all cases. In a certain limiting case, namely temporally decorrelated (rapidly varying) flows, exact, analytical expressions exist for the mean growth rate. Using numerical simulations, we assess the extent to which our model applies to real mixing protocols, and map the stochastic parameters on to flow parameters.

1. Introduction

When a passive tracer is stirred by a flow that varies rapidly in space and time, stochastic models are often used to describe the mixing [1]. Based on the Fokker–Planck (FP) equation, we develop a model for the probability distribution function (PDF) of the growth rate of the tracer gradient in a generic, two-dimensional flow that varies on arbitrary timescales. In this introduction, we place our model in the context of existing literature.

Kraichnan [2] modelled homogeneous isotropic turbulence as Gaussian fluctuations. In this description, the PDF for the largest finite-time Lyapunov exponent can be found using the Central Limit Theorem. The same model has been used to describe the so-called strange eigenmode [3] in passive-tracer decay [4]. Balkovsky and Fouxon [5] generalised the Kraichnan model to account for temporally correlated flows. When the correlation time tends to zero, their analysis yields the PDF of all the finite-time Lyapunov exponents (in an arbitrary number of spatial dimensions) [5,6]. For a review of these techniques, see [1]. In the present work, we focus instead on the distribution of the growth rate of the tracer gradient, a distinct but related quantity.

In the limit of zero diffusion, the problem of determining the growth rate of a passive-tracer gradient is identical to the study of the growth rate of a material line [7]. The latter has been studied extensively, with particular emphasis on the inverse relationship between the magnitude of material-line curvature and the growth rate [8–11]. The passive-tracer gradient dynamics are also similar to the kinematic dynamo in magnetohydrodynamics [12]. Indeed, our starting point for the derivation of the orientation dynamics of the tracer gradient is an equation that is identical in form to the evolution equation for the magnetic field. Our focus however, is on purely two-dimensional systems.

In this two-dimensional context, Lapeyre et al. [13] derived a pair of equations to describe the growth rate of the gradient of a passively advected tracer. The theory is based on the orientation of the tracer gradient relative to the straining (compressive) direction of the flow: if the tracer gradient aligns with the compressive direction, it blows up. However, the tracer-gradient orientation is instead fixed by a balance between strain and 'effective' vorticity (the sum of vorticity and twice the rotation rate of the strain eigenbasis). Thus, blow-up is prevented in rotation-dominated regions. The inclusion of the rotation rate generalises the description of orientation dynamics implied by the Okubu–Weiss criterion [14]. That said, the Lapeyre criterion relies on the adiabatic approximation of the differential equations: the effective vorticity and strain eigenvalue are assumed to vary slowly along trajectories. Although this description is valid in certain cases (e.g. [15]), it may not hold when the stirring flow is governed by some kind of externally imposed, rapidly varying forcing: this will be our focus herein.

Gonzalez and Paranthoën [16] studied two mixing protocols wherein the adiabatic assumption breaks down. They show numerically that the tracer gradient points in a direction fixed by the average value of the ratio r of effective vorticity to strain. Garcia

* Tel.: +353 1 716 2546; fax: +353 1 716 1172.
E-mail address: lennon.onaraigh@ucd.ie.

0997-7546/$ – see front matter © 2010 Elsevier Masson SAS. All rights reserved.
doi:10.1016/j.euromechflu.2010.10.001

et al. [17] introduced a stochastic model of such scenarios by regarding r as the solution to a stochastic differential equation (SDE). They found good agreement with an experiment they performed. However, they neither examined the distribution of growth rates of the tracer gradient elicited by this model (but see [18]), nor analysed the associated FP equation. Further studies by other authors [19,20] have involved the FP equation of alignment dynamics for simple shear flows; our work can be regarded as building on this approach. Thus, in the present work, we provide a detailed model of a generic flow (Section 3), and we make the connection with the FP equation [21], an approach that facilitates fast, accurate numerical calculations, analytical results, and highlights the striking analogies between the current work and a variety of other physical systems [21]. Furthermore, our approach involves a comparison between theoretical models and simulations of the random-phase sine flow (Section 4), and forced, two-dimensional turbulence (Section 5), an exercise that strengthens the case for the model developed herein. First, we review the orientation dynamics derived elsewhere [13,22].

2. The orientation dynamics

The description of the orientation dynamics starts with the vector field $\boldsymbol{\mathcal{B}} = (-\theta_y, \theta_x)$, where θ is the passively advected tracer

$$\theta_t + \boldsymbol{u}\cdot\nabla\theta = \kappa\Delta\theta, \qquad \nabla\cdot\boldsymbol{u} = 0. \tag{1}$$

In this section, we take the molecular diffusivity κ to be zero; we study the implications of finite κ-values at the end of the derivation. When $\kappa = 0$, the vector $\boldsymbol{\mathcal{B}}$ satisfies the material-line equation

$$\boldsymbol{\mathcal{B}}_t + \boldsymbol{u}\cdot\nabla\boldsymbol{\mathcal{B}} = \boldsymbol{\mathcal{B}}\cdot\nabla\boldsymbol{u}. \tag{2}$$

This result can be obtained by brute-force calculation based on Eq. (1), or by other means.[1] Our study uses this indirect approach (rather than writing down a partial differential equation for $\nabla\theta$) because the resulting equation fits into the general framework of stretching dynamics described in the paper of Gibbon and Holm [23], which encompasses three-dimensional vorticity, and magnetohydrodynamics. The modelling insights developed in the present work may help to shed some light on these more difficult problems. We take the dot product of Eq. (2) with $\boldsymbol{\mathcal{B}}$ itself; the result is diagonalisable in terms of real eigenvalues:

$$\frac{\mathrm{d}}{\mathrm{d}t}|\boldsymbol{\mathcal{B}}|^2 = 2\left(\mathcal{B}_1, \mathcal{B}_2\right)\begin{pmatrix} s & d \\ d & -s\end{pmatrix}\begin{pmatrix}\mathcal{B}_1 \\ \mathcal{B}_2\end{pmatrix}. \tag{3}$$

The rate-of-strain matrix S appears in Eq. (3): $s = u_x$ and $d = \left(u_y + v_x\right)/2$. We identify $\beta - (\pi/2)$ as the phase of the vector $\boldsymbol{\mathcal{B}}$, where $\tan\beta = \theta_y/\theta_x$, and obtain, by means similar to before, an equation for β:

$$\frac{\mathrm{d}\beta}{\mathrm{d}t} = \frac{1}{2}\omega - \frac{1}{|\boldsymbol{\mathcal{B}}|^2}\left(\mathcal{B}_2, -\mathcal{B}_1\right)\begin{pmatrix} s & d \\ d & -s\end{pmatrix}\begin{pmatrix}\mathcal{B}_1 \\ \mathcal{B}_2\end{pmatrix}, \tag{4}$$

where $\omega = v_x - u_y$ is the vorticity. To complete our analysis, we re-write Eq. (3) in terms of the eigenvalues of S:

$$\frac{\mathrm{d}}{\mathrm{d}t}|\boldsymbol{\mathcal{B}}|^2 = -\left(2\mu\sin\zeta\right)|\boldsymbol{\mathcal{B}}|^2. \tag{5}$$

We define an eigenbasis $\boldsymbol{X}_{(+)}$ and $\boldsymbol{X}_{(-)}$ such that the vector $\boldsymbol{X}_{(+)}$ lies in the positive quadrant. The associated eigenvalue is non-sign-definite, $\mu = \mathrm{sign}(d)\sqrt{s^2+d^2}$. This enables us to decompose the strain rate μ into a mean part and a fluctuation. The angle between the x-axis and $\boldsymbol{X}_{(+)}$ is φ, and $\zeta = 2\left(\beta - \varphi + \frac{1}{4}\pi\right)$. Hence, from Eq. (4)

$$\frac{\mathrm{d}\zeta}{\mathrm{d}t} = -2\mu\cos\zeta + \omega - 2\frac{\mathrm{d}\varphi}{\mathrm{d}t}. \tag{6}$$

We also identify the growth rate of the gradient:

$$\Lambda := -2\mu\sin\zeta. \tag{7}$$

The angle φ gives the orientation of the expansive eigenvector if $d > 0$ and gives the orientation of the compressive direction otherwise. The character of this direction is therefore indeterminate, and the dynamics of the angle ζ apparently fail to tell us whether the tracer gradient aligns with the compressive axis. However, we can demonstrate that if the most probable values of ζ are $\pm\pi/2$, then the tracer gradient aligns with the compressive direction, in an average sense. First, define the angle

$$\varphi_{\mathrm{comp}} = \varphi - \frac{1}{2}\pi H\left(\mu\right),$$

where $H(\cdot)$ is the Heaviside step function; then φ_{comp} is always the angle between the x-axis and the compressive direction. Next, define a new angle

$$\zeta_{\mathrm{comp}} = 2\left(\beta - \varphi_{\mathrm{comp}} + \frac{1}{4}\pi\right),$$

such that $\zeta_{\mathrm{comp}} - \pi H\left(\mu\right) = \zeta$. Alignment of the tracer gradient with the compressive direction corresponds to $\beta = \varphi_{\mathrm{comp}}$, or $\zeta_{\mathrm{comp}} = \pi/2$. The growth rate $\Lambda = -2\mu\sin\zeta$ is now re-expressed as

$$\Lambda = 2|\mu|\sin\zeta_{\mathrm{comp}}.$$

Finally, the instantaneous deviation Δ of the system away from the compressive direction is given by $\Delta = \zeta_{\mathrm{comp}} - (\pi/2)$, or

$$\Delta = \zeta + \pi\left[H\left(\mu\right) - \frac{1}{2}\right]. \tag{8}$$

In order for the tracer gradient to align with the compressive direction in an average sense, the PDF of Δ must have a maximum at zero. Equivalently, the PDF of ζ must have maxima at $\pm\pi/2$.

The basic equations (3) and (6) rely only on the assumptions $\kappa = 0$ and incompressibility. For small but finite κ-values (nondimensionalised relative to appropriate scales of length and time), the main effect of diffusion is to reduce the growth rate of the gradient, through the presence of a negative-definite term in Eq. (5) [18]. The quantity Λ loses its identity as the growth rate of the tracer gradient and becomes the *production rate* of gradient. Nevertheless, it is still legitimate to study this quantity: merely its role changes, and the orientation dynamics are not modified [13]. On the other hand, for large κ-values, the orientation dynamics are affected: there is a competition between nonlinear diffusion, which promotes alignment with the direction of large gradients, and linear diffusion, which 'smears out' the preferred direction [24]. The nonlinear diffusion arises from the coupling of orientation angles and tracer-gradient magnitudes which occurs when $\nabla\theta$ is written in $(|\boldsymbol{\mathcal{B}}|, \beta)$ variables. In this work the focus is on the former case (small diffusivity), and our numerical simulations in Section 5 suggest a negligible role for diffusion in the orientation dynamics.

3. A stochastic model

In this section we formulate a closure model for the forces in the equation for the dynamics of the angle ζ. Although the variables denoting the compressional direction introduced in Section 2

[1] Indeed, one may regard $\boldsymbol{\mathcal{B}}$ as a complex-valued two-form $\mathcal{B} = \mathcal{B}_1 + \mathrm{i}\mathcal{B}_2$ and operate on both sides of the two-form identity $\mathcal{B}\mathrm{d}z\wedge\mathrm{d}\bar{z} = 2\mathrm{i}\mathrm{d}z\wedge\mathrm{d}\theta$ with the material derivative.

are more physical, the use of the quantities ζ and μ facilitates a decomposition of the forces into mean and fluctuating components. Thus, we re-write Eq. (6):

$$\frac{1}{2}\frac{\mathrm{d}X}{\mathrm{d}t} = (-\mu_0 \cos X + w) - Y(t)\cos X + Z(t), \tag{9a}$$

(for notational reasons [21], we write $X := \zeta$), where $\mu = \mu_0 + Y(t)$ and $(\omega/2) + \dot{\varphi} = w + Z_0(t)$ represent decompositions into mean components and fluctuations. Homogeneity and isotropy of the flow imply that $\langle \mu \rangle = \mu_0 = 0$. Similarly, homogeneity, isotropy, and the boundedness $0 \leq \varphi \leq \pi/2$ imply that $\langle \dot{\varphi} \rangle = 0$. Thus, the mean value of the effective vorticity is independent of the rotation rate of the strain eigenbasis, $\langle w \rangle = \langle \omega \rangle/2$. We model the fluctuations as Ornstein–Uhlenbeck (OU) processes, with mean zero, decay times τ_Y and τ_Z, and strengths D_Y and D_Z respectively (the fluctuations reduce to Wiener processes in the limit where the decay times tend to zero). We anticipate this model to be appropriate in particular when the flow is governed by some random, externally prescribed stirring mechanism (for examples, see [25]). Thus, the noise terms satisfy the following equations:

$$\mathrm{d}Y = -\frac{Y}{\tau_Y}\mathrm{d}t + \sqrt{\frac{2\sigma_Y^2}{\tau_Y}}\mathrm{d}W_Y, \tag{9b}$$

$$\mathrm{d}Z = -\frac{Z}{\tau_Z}\mathrm{d}t + \sqrt{\frac{2\sigma_Z^2}{\tau_Z}}\mathrm{d}W_Z + \sqrt{\frac{2k^2}{\tau_Z}}\mathrm{d}W_Y, \tag{9c}$$

where $\mathrm{d}W_Y$ and $\mathrm{d}W_Z$ are uncorrelated Wiener processes, $\langle \mathrm{d}W_{Y,Z} \rangle = 0$, $\langle \mathrm{d}W_{Y,Z}^2 \rangle = \mathrm{d}t$. For generality, and because the forces Y and Z come from the same underlying flow, we assume a cross-correlation $k \neq 0$. The following correlation relations follow from Eq. (9):

$$\langle Y(t)Y(t') \rangle = \frac{D_Y}{\tau_Y}\mathrm{e}^{-|t-t'|/\tau_Y}, \qquad \langle Z(t)Z(t') \rangle = \frac{D_Z}{\tau_Z}\mathrm{e}^{-|t-t'|/\tau_Z},$$

together with the cross-correlation

$$\langle Y(t)Z(t') \rangle = \frac{2c\sqrt{D_Y D_Z}}{\tau_Y + \tau_Z}\mathrm{e}^{-|t-t'|/\left(H(t-t')\tau_Y + H(t'-t)\tau_Z\right)},$$

where $H(\cdot)$ is the Heaviside step function, and

$$\sigma_Y^2 = \frac{D_Y}{\tau_Y}, \qquad \sigma_Z^2 + k^2 = \frac{D_Z}{\tau_Z}, \qquad c^2 = \frac{k^2\tau_Z}{D_Z},$$

with $c^2 \leq 1$. In Sections 4 and 5 we discuss strategies for choosing the parameters $(D_Y, D_Z, \tau_Y, \tau_Z, c)$ so as to maximise the overlap between our model and real flow protocols. Note that these temporal correlations converge to delta functions as $\tau_Y, \tau_Z \to 0$. Finally, we make the assumption that the underlying, noise-generating flow is homogeneous in space in a statistical sense:

$$\left\langle Y\left(t; \boldsymbol{x}_0\right) Y\left(t'; \boldsymbol{x}_0'\right) \right\rangle = \tau_Y^{-1}\mathcal{D}_Y\left(\boldsymbol{x}_0 - \boldsymbol{x}_0'\right)\mathrm{e}^{-|t-t'|/\tau_Y}, \quad \&\mathrm{c}.$$

Hence,

$$\left\langle Y\left(t; \boldsymbol{x}_0\right) Y\left(t'; \boldsymbol{x}_0\right) \right\rangle = \tau_Y^{-1}\mathcal{D}_Y(0)\mathrm{e}^{-|t-t'|/\tau_Y} := \tau_Y^{-1}D_Y\mathrm{e}^{-|t-t'|/\tau_Y}, \quad \&\mathrm{c}.,$$

and the noise strength is independent of the initial position of the Lagrangian particle.

Eq. (9) is Markovian with uncorrelated noise terms if viewed in an augmented state space (X, Y, Z). We nondimensionalise this equation set on the timescale D_Y^{-1}. In scaled variables, Eq. (9) reads

$$\mathrm{d}X = 2\left(\tilde{w} - \tilde{Y}\cos X + \tilde{Z}\right)\mathrm{d}\tilde{t}, \tag{10a}$$

$$\mathrm{d}\tilde{Y} = -\frac{\tilde{Y}}{\tilde{\tau}_Y}\mathrm{d}\tilde{t} + \frac{\sqrt{2}}{\tilde{\tau}_Y}\mathrm{d}\tilde{W}_{\tilde{Y}}, \tag{10b}$$

$$\mathrm{d}\tilde{Z} = -\frac{\tilde{Z}}{\tilde{\tau}_Z}\mathrm{d}\tilde{t} + \frac{\sqrt{2\rho\left(1-c^2\right)}}{\tilde{\tau}_Z}\mathrm{d}\tilde{W}_{\tilde{Z}} + \frac{\sqrt{2c^2\rho}}{\tilde{\tau}_Z}\mathrm{d}\tilde{W}_{\tilde{Y}}, \tag{10c}$$

where

$$\left(\tilde{t}, \tilde{\tau}_Y, \tilde{\tau}_Z, \tilde{w}, \tilde{Y}, \tilde{Z}, \rho\right) = \left(tD_Y, \tau_Y D_Y, \tau_Z D_Y, w/D_Y, Y/D_Y, Z/D_Y, D_Z/D_Y\right),$$

and where $\langle \mathrm{d}\tilde{W}_{\tilde{Y},\tilde{Z}}^2 \rangle = \mathrm{d}\tilde{t}$. Following standard practice, in the rest of this section we work only with the nondimensional equations and drop the ornamentation over the scaled variables. The form of Eq. (10a) is identical to descriptions of pendulum motion in the overdamped limit, the orientation of electric dipoles in an external field, and the Josephson junction [26,27], while the form of Eqs. (10a)–(10c) is similar to a semiclassical model of lasers [21].

The probability that the triple of observables (X, Y, Z) is contained in an interval $(x \leq X \leq x + \mathrm{d}x, y \leq Y \leq y + \mathrm{d}y, z \leq Z \leq z + \mathrm{d}z)$ at time t is given by $P_{XYZ}(x, y, z, t)\,\mathrm{d}x\,\mathrm{d}y\,\mathrm{d}z$. Knowledge of this function enables us to compute the PDF of angles X, and growth rates Λ. These are marginal PDFs that can be derived from the PDF $P_{XYZ}(x, y, z, t)$, which satisfies the following FP equation (we omit the subscript on P_{XYZ}):

$$\frac{\partial P}{\partial t} = \mathcal{L}_{\mathrm{OU}}P - \frac{\partial}{\partial x}(VP), \tag{11}$$

where

$$\mathcal{L}_{\mathrm{OU}} = \frac{1}{\tau_Y}\frac{\partial}{\partial y}(y\,\circ) + \frac{1}{\tau_Y^2}\frac{\partial^2}{\partial y^2} + \frac{1}{\tau_Z}\frac{\partial}{\partial z}(z\,\circ) + \frac{\rho}{\tau_Z^2}\frac{\partial^2}{\partial z^2} + \frac{2c\rho^{1/2}}{\tau_Y\tau_Z}\frac{\partial^2}{\partial y\partial z} \tag{12}$$

is the OU operator associated with the $Y - Z$ observables, and

$$V(x, y, z) = 2(w - y\cos x + z)$$

is the drift velocity. We solve the *stationary* FP equation with $x \in [-\pi, \pi]$ and $y, z \in (-\infty, \infty)$. The PDF of angles is obtained from the stationary solution $P(x, y, z)$:

$$P_X(x) = \int_{-\infty}^{\infty}\int_{-\infty}^{\infty} P(x, y, z)\,\mathrm{d}y\,\mathrm{d}z.$$

Finally, the PDF of growth rates $\Lambda = -2Y\sin X$ is computed through a coordinate transformation of the y-variable:

$$\mathrm{Prob}(\lambda \leq \Lambda \leq \lambda + \mathrm{d}\lambda) = P_\Lambda(\lambda)\,\mathrm{d}\lambda = \left[\int_{-\pi}^{\pi} P_{XY}\left(x, \frac{\lambda}{-2\sin x}\right)\frac{1}{2|\sin x|}\mathrm{d}x\right]\mathrm{d}\lambda, \tag{13}$$

and this transformation is legitimate because the Jacobian diverges only where P vanishes, and P vanishes rapidly as $y \to \pm\infty$. Before describing these equations in full generality, we focus on two special cases, one of which admits analytical solutions.

Case 1: *The rate of strain Y varies slowly*: In this limit, $\tau_Y \to \infty$. We investigate the extent to which this extreme case corresponds to the adiabatic model of Lapeyre [13]. We set $Y = 1$, $c = 0$, and the FP equation to solve is

$$\frac{\partial P}{\partial t} = \frac{\rho}{\tau_Z^2}\frac{\partial^2 P}{\partial z^2} + \frac{1}{\tau_Z}\frac{\partial}{\partial z}(zP) - \frac{\partial}{\partial x}\left[2(w + z - \cos x)P\right]. \tag{14}$$

For this special case, Eq. (8) implies that alignment of the tracer gradient with the compressive direction occurs when $X = -\pi/2$. Moreover, since Y is equal to one, $\Lambda = -2\sin X$, and explosive growth in the tracer gradient is synonymous with its alignment along the compressive direction. Sample equilibrium solutions of Eq. (14) are shown in Fig. 1. The PDF has a single maximum in all cases. However, the location of the maximum changes as a function both of the effective rotation w, and the diffusion strength ρ: at fixed diffusion strength, and as w increases, the location of the maximum shifts from $x = -\pi/2$ at $w = 0$, to $x = 0$ at $w = \infty$

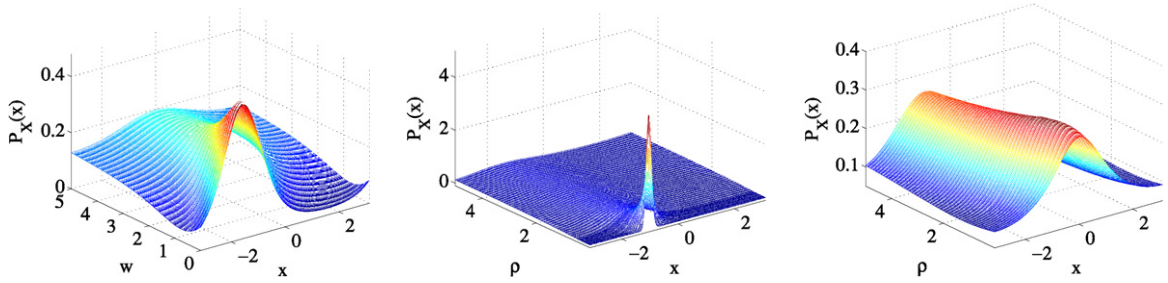

(a) $\rho = \tau_Z = 1$. (b) $w = 0.5$, $\tau_Z = 1$. (c) $w = 2$, $\tau_Z = 1$.

Fig. 1. Sample PDFs in the limit where the strain Y is constant.

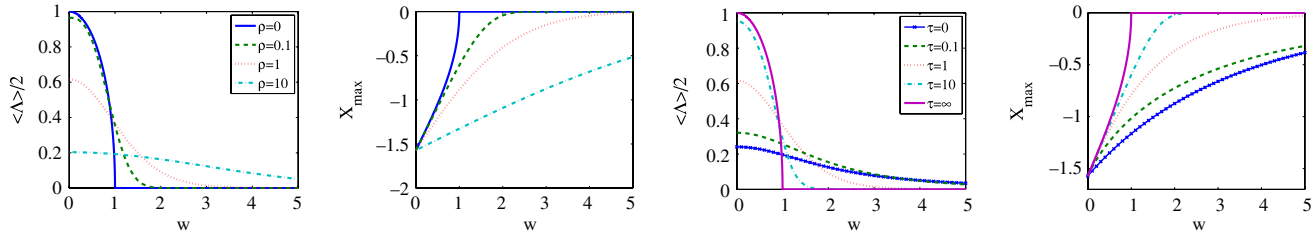

(a) $\tau_Z = 1$. (b) $\tau_Z = 1$. (c) $\rho = 1$. (d) $\rho = 1$.

Fig. 2. Parameter study in the limit $\tau_Y \to \infty$. (a), (b) the effect of varying the noise strength ρ; (c), (d) the effect of varying the relaxation time τ_Z.

(Fig. 1(a)). At fixed $w < 1$, and as ρ increases, the location of the maximum shifts from $x = -\pi/2$ at $\rho = 0$ to more negative values. Similarly, at fixed $w > 1$, the location of the maximum shifts from $x = 0$ at $\rho = 0$ to more negative values. In Fig. 2 we present further results from the equilibrium PDFs based on expectation values. Fig. 2(a)–(b) are the counterpart to Fig. 1(b)–(c), wherein ρ is varied. In these cases, setting $\rho = 0$ yields the deterministic PDF [21]

$$P_X(x) = \begin{cases} \delta(x - x_0), & x_0 = -\cos^{-1}(w), \quad w \le 1, \\ \dfrac{1}{2\pi}\dfrac{\sqrt{w^2-1}}{w - \cos(x)}, & w > 1, \end{cases} \tag{15}$$

such that $X_{\max} = \langle X \rangle = x_0$ for $w \le 1$. Therefore, for the case (15), increasing the level of effective vorticity from zero forces the tracer gradient out of alignment with the compressive direction until a rotational state is reached ($w = 1$), wherein the angle X rotates constantly, to give a preferred value of zero. Exponential growth ($\langle \Lambda \rangle > 0$) is possible for Eq. (15) only when $w < 1$. The parametric dependence of the statistics on w is similar at finite values of diffusion. However, the mean growth rate is positive for all finite (ρ, w)-values, and explosive growth in the tracer gradient always happens. Fig. 2(a)–(b) can also be understood using a particle analogy: $\mathcal{U}(X) = 2\sin(X)$ is a potential well, and a fictitious particle undergoes the dynamics $\dot{X} = -\mathcal{U}'(X) + 2w + 2Z(t)$. For $w < 1$, the potential well has a minimum when $X = x_0$, which in the absence of noise, is the preferred state. However, the noise $Z(t)$ forces the particle away from this state, such that the favoured location of the particle is no longer x_0. As the noise increases in strength, the particle wanders (on average) further and further away from x_0, and the preferred state drifts away from x_0. This particle analogy is also helpful in the next limiting case we consider (Case 2).

In Fig. 2(c)–(d) we vary τ_Z. The case $\tau_Z = \infty$ again leads to deterministic behaviour, given by Eq. (15). This case is also identical to the adiabatic scenario described by Lapeyre. For finite values of the relaxation time, the maximum value of the PDF no longer tends sharply to zero for $w > 1$, but rather tends smoothly to zero as $w \to \infty$. Thus, the mean growth rate is less than the adiabatic value for $w < 1$ and exceeds the adiabatic value for $w > 1$, and exponential growth of the tracer gradient always happens. The case $\tau_Z \to 0$ is also shown in these figures, and is qualitatively similar to the finite-τ_Z case. We now examine this limiting situation in more detail.

Case 2: *The forcing terms Y and Z vary rapidly*: In this limit, the rate of strain and the effective vorticity vary rapidly, and $\tau_Y = \tau_Z = \tau \to 0$. An explicit formula for the PDF of angles exists (up to quadratures). This enables us to prove some rigorous results concerning the orientation of the tracer gradient relative to the compressive direction; it also facilitates a detailed parameter study to investigate whether the mean growth rate is always positive. First, because $\tau_Y = \tau_Z := \tau$, we re-write the model (10) as

$$\mathrm{d}X = 2\left[w + \left(-\cos X + c\rho^{1/2}\right)Y + Z_1\right]\mathrm{d}t, \tag{16a}$$

$$\mathrm{d}Y = -\frac{Y}{\tau}\mathrm{d}t + \frac{\sqrt{2}}{\tau}\mathrm{d}W_Y, \tag{16b}$$

$$\mathrm{d}Z_1 = -\frac{Z_1}{\tau}\mathrm{d}t + \frac{\sqrt{2\rho\left(1-c^2\right)}}{\tau}\mathrm{d}W_Z, \tag{16c}$$

where $Z_1 = Z - c\rho^{1/2}Y$, and $\langle YZ_1 \rangle = 0$. (Henceforth, unless otherwise indicated, we work with the variables (X, Y, Z_1) and omit the subscript on Z_1. The distinction between the variables (X, Y, Z) and (X, Y, Z_1) vanishes when $c = 0$.) We take the limit $\tau \to 0$ and solve the associated Fokker–Planck equation for the stationary PDF of angles $P(x)$:

$$J = A(x)P(x) - \frac{\mathrm{d}}{\mathrm{d}x}\left[P(x)B(x)\right], \tag{17}$$

where J is the constant probability current and in the Stratonovich interpretation, the coefficients A and B have the following form:

$$A(x) = w + g'(x)\left[g(x) + c\rho^{1/2}\right],$$

$$B(x) = \rho\left(1 - c^2\right) + \left[g(x) + c\rho^{1/2}\right]^2,$$

where $g(x) = -\cos x$. Introducing the effective potential

$$\mathcal{U}_{\mathrm{eff}}(x) = -\int_{-\pi}^{x} \frac{A\left(x'\right)}{B\left(x'\right)}\mathrm{d}x',$$

$$P(x) = \frac{1}{B(x)}\mathrm{e}^{-\mathcal{U}_{\mathrm{eff}}(x)}\left[N - J\int_{-\pi}^{x}\mathrm{e}^{\mathcal{U}_{\mathrm{eff}}(x')}\mathrm{d}x'\right], \tag{18}$$

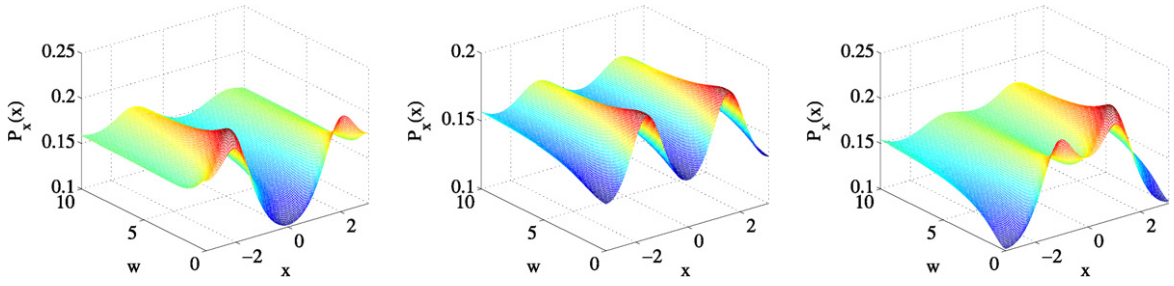

(a) $c = -0.5$. (b) $c = 0$. (c) $c = 0.5$.

Fig. 3. The PDF $P(x)$ for the rapidly forced case. The PDF has a single global maximum for $c \neq 0$: for positive c-values, the maximum occurs at positive angles, and vice versa. For $c = 0$, the PDF has two identical global maxima. Increasing w produces less pronounced maxima.

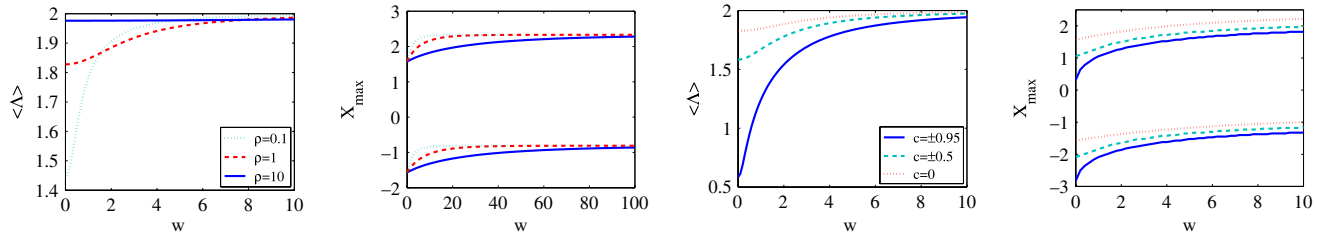

(a) $c = 0$. (b) $c = 0$. (c) $\rho = 1$. (d) $\rho = 1$.

Fig. 4. Parameter studies of the mean growth rate $\langle \Lambda \rangle$ and the angle $X_{\max}$ that maximises the PDF (rapidly forced case). The mean growth rate is positive in each case considered. (a), (b) The effects of varying w and ρ; (c), (d) the effects of varying w and c. Changing the sign of c does not affect the mean growth rate although it does change the location and sign of the PDF maximum: it is negative for $c < 0$ and positive for $c > 0$. For $c = 0$ there are two maxima at positive and negative locations.

where N and J are constants of integration fixed by normalisation and by the periodicity condition

$$J = \frac{B(-\pi)P(-\pi)\left[e^{\mathcal{U}_{\text{eff}}(-\pi)} - e^{\mathcal{U}_{\text{eff}}(\pi)}\right]}{\int_{-\pi}^{\pi} e^{\mathcal{U}_{\text{eff}}(x)} dx}, \tag{19}$$

where w and c are not both zero (this degenerate case is discussed below). Thus, $P(x)$ is 2π-periodic on $[-\pi, \pi]$ [21,26]. Sample PDFs are shown in Fig. 3. An expression for the *mean* growth rate $\langle \Lambda \rangle = -\langle 2Y \sin X \rangle$ now follows from an application of the Forutsu–Novikov theorem [28,26]:

$$\langle Y(t) g^{(n)}(X) \rangle = 2 \int_{-\infty}^{\infty} \delta(t - t') \left\langle g^{(n+1)}(X(t')) \left[g(X(t')) + c\rho^{1/2} \right] \right\rangle dt'.$$

Setting $n = 1$ gives

$$\langle \Lambda \rangle = 4\left(\langle \cos^2 X \rangle - c\rho^{1/2} \langle \cos X \rangle \right). \tag{20}$$

Three analytical results arise from this formalism:

1. If $w = 0$, the maxima of $P(x)$ lie at $x = \pm\pi/2$, and the tracer gradient aligns with the compressive direction, on average (Eq. (18));
2. If $c = 0$, the mean growth rate is definitely non-negative (Eq. (20));
3. If $w = c = 0$, it follows that $J = 0$. Thus, $P(x) \propto B(x)^{-1/2}$, and using Eq. (20),

$$\langle \Lambda \rangle = 4\rho \left[\left(1 + \frac{1}{\rho} \right) \frac{E\left(\pi \middle| \frac{1}{\rho+1} \right)}{F\left(\pi \middle| \frac{1}{\rho+1} \right)} - 1 \right], \tag{21}$$

where E and F are incomplete elliptic functions of the first and second kinds, respectively.

To study more cases, we turn to the results in Fig. 4, where we focus on three parameters, w, ρ, and c. The mean growth rate $\langle \Lambda \rangle$ is positive in all of the parameter studies, and is independent of the sign of c. In contrast to Case 1, the mean growth rate is an *increasing* function of w. This can be understood from the particle analogy employed previously: for large w-values, the fictitious particle wanders freely through the whole domain, and the PDF of particle locations tends to a constant. However, the particle location and the Y-values are correlated, through the Furutsu–Novikov theorem, and hence $\langle \Lambda \rangle \sim 4\int_{-\pi}^{\pi} \cos^2(x)\, dx/(2\pi) = 2$. We have verified this finding further by solving the SDE (16) directly (with $\tau = 0$): the mean growth rate computed over an ensemble of trajectories coincides with the value given by the Furutsu–Novikov theorem. We have also solved the FP equation associated with Eq. (16) for various τ-values: as τ is decreased, the w-dependence of the mean growth rate switches from monotonically decreasing to monotonically increasing, and agrees with the white-noise case in the limit as $\tau \to 0$. In sum, this effect is confined to the near-white-noise region.

In the final numerical study, we generate some sample numerical results concerning the marginal PDFs for arbitrary parameter values. We focus on cases where the stirring is intermediate between rapid and slow, that is, τ_Y and τ_Z are $O(1)$ in the nondimensional units. We have carried out several studies for different c- and w-values. Our numerical results demonstrate that for $w = 0$, the PDF $P_X(x)$ has maxima at $x = \pm\pi/2$. These results are not shown here, but are shown in Sections 4 and 5. Instead, in the remainder of this section, we focus on $\tau_Y = \tau_Z$, $w \neq 0$, and $c \neq 0$ (Figs. 5 and 6). The diffusion equation associated with Eqs. (16) is solved using a semi-implicit spectral method; as a validation of our technique, we compute the marginal PDF P_{YZ}. Since Y and Z are independent OU processes, we must have

$$P_{YZ}(y, z) = \int_{-\pi}^{\pi} P(x, y, z)\, dx \propto e^{-y^2\tau_Y/2} e^{-z^2\tau_Z/\left[2\rho\left(1-c^2\right)\right]}. \tag{22}$$

Our numerical results are indeed Gaussian (Fig. 5), with decay scales in agreement with Eq. (22). Thus, we are satisfied with the accuracy of the method. The PDF of angles X is computed from the full solution $P(x, y, z)$ using numerical integration: this is asymmetric around $x = 0$, with maxima to the right of $x = \pm\pi/2$. The shift in the maxima away from $\pm\pi/2$ is due to the finite value of

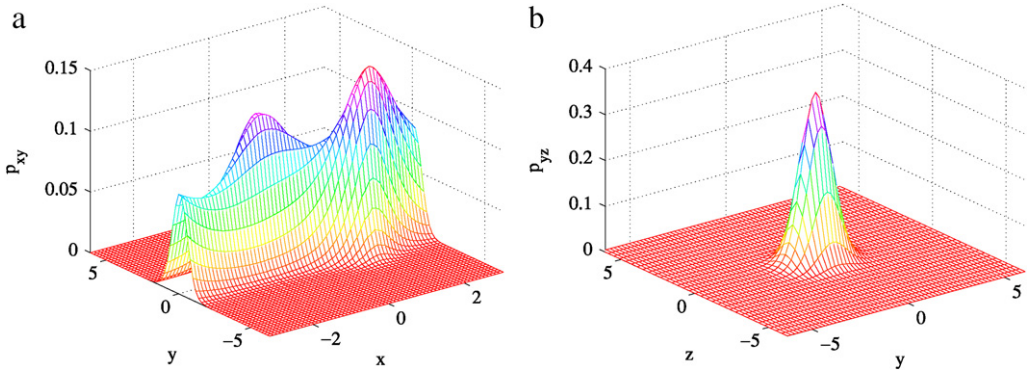

Fig. 5. Marginal probability distributions obtained from the stationary FP equation. (a) The distribution in x–y space; (b) The distribution in y–z space. The latter is Gaussian, with decay scales in agreement with the theoretical values in Eq. (22). Here $w = c = 0.5$, $\rho = 1$, and $\tau_Y = \tau_Z = 2$.

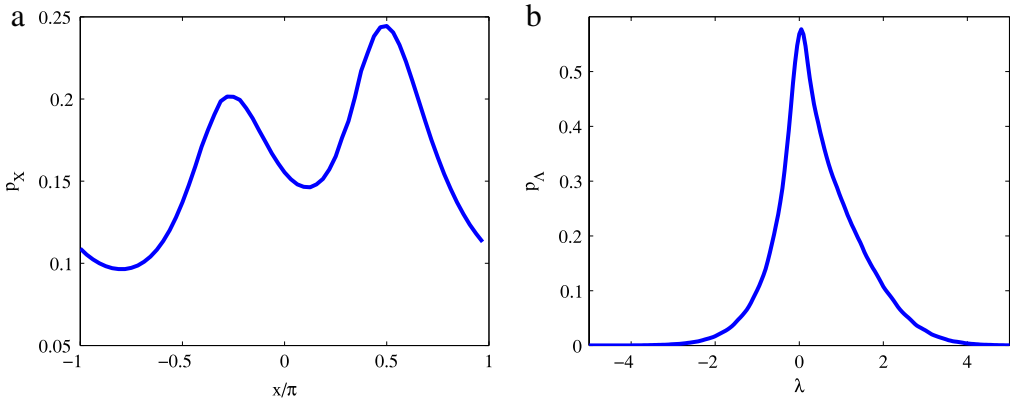

Fig. 6. (a) The PDF of angles according to the SDE (16), for nonzero values of w and c. (b) The PDF of growth rates. A clear preference for positive growth is present. Here $w = c = 0.5$, $\rho = 1$, and $\tau_Y = \tau_Z = 2$.

w in the calculation, while the asymmetry in the maxima is due to the finite value of the correlation coefficient c. The shift in the maxima means that the tracer gradient does not align with the compressive direction (Eq. (8)). However, the mean growth rate of the tracer gradient is positive, since the distribution of growth rates is skewed (Fig. 6(b)). This suggests the favoured orientation and the compressive direction, although distinct, are close in value. Our results correspond to the situation described by Gonzalez and Paranthoën [16] for rapidly varying flows, where the tracer gradient aligns with a direction fixed by the mean value $\langle r \rangle$; this coincides with the compressive direction only when $\langle r \rangle = 0$. We now compare the analytical results of the model with numerically simulated flows.

4. The random-phase sine flow

In this section we compute the orientation statistics for the random-phase sine flow [3,29]. This flow is amenable to a comparison with our stochastic model because the randomisation of the phases breaks the invariant tori, induces homogeneity, and promotes mixing [30]. This is in contrast to the unrandomised sine flow studied elsewhere [16].

The flow is quasi-periodic and is defined as follows. In the jth period,

$$u = A_0 \sin\left(ky + \phi_j\right), \qquad v = 0, \tag{23a}$$

for the first half-period, and

$$u = 0, \qquad v = A_0 \sin\left(kx + \psi_j\right) \tag{23b}$$

for the second. Here τ is the period of the flow, A_0 is the flow amplitude, and ϕ_j and ψ_j are random phases that are updated once per period.

In the jth cycle of the sine flow, the strain and the vorticity have the form

$$\begin{aligned} d &= \frac{1}{2}A_0 k H_\tau(t)\cos\left(ky + \phi_j\right) \\ &\quad + \frac{1}{2}A_0 k\left(1 - H_\tau(t)\right)\cos\left(kx + \psi_j\right), \end{aligned} \tag{24a}$$

$$\begin{aligned} \omega &= -A_0 k H_\tau(t)\cos\left(ky + \phi_j\right) \\ &\quad + A_0 k\left(1 - H_\tau(t)\right)\cos\left(kx + \psi_j\right), \end{aligned} \tag{24b}$$

where $H_\tau(t)$ is equal to unity in the first half-period and is zero in the second. Eqs. (24) imply that d and ω are not correlated with each other, and that their autocorrelation functions are nonzero only in a half-period, wherein they take constant values. Furthermore, since $\varphi = \text{Const.}$ for the sine flow,

$$\left(\partial_t + \boldsymbol{u}\cdot\nabla\right)X = \omega - 2d\cos X, \tag{25}$$

where $X = 2\left(\beta - \varphi + \frac{1}{4}\pi\right) = 2\beta$. We substitute the definitions of the strain d and the vorticity ω (Eqs. (24)) into Eq. (25). Along a trajectory with coordinates $\left(x_{j+1}, y_j\right)$ in the first half-period and $\left(x_{j+1}, y_{j+1}\right)$ in the second, Eq. (25) reads

$$\begin{aligned} \frac{\mathrm{d}}{\mathrm{d}t}X\left(x_{j+1}, y_j\right) &= -A_0 k\cos\left(ky_j + \phi_j\right) \\ &\quad - A_0 k\cos\left(ky_j + \phi_j\right)\cos X\left(x_{j+1}, y_j\right), \end{aligned} \tag{26}$$

in the first half-period and

$$\begin{aligned} \frac{\mathrm{d}}{\mathrm{d}t}X\left(x_{j+1}, y_{j+1}\right) &= A_0 k\cos\left(kx_{j+1} + \psi_j\right) \\ &\quad - A_0 k\cos\left(kx_{j+1} + \psi_j\right)\cos X\left(x_{j+1}, y_{j+1}\right), \end{aligned} \tag{27}$$

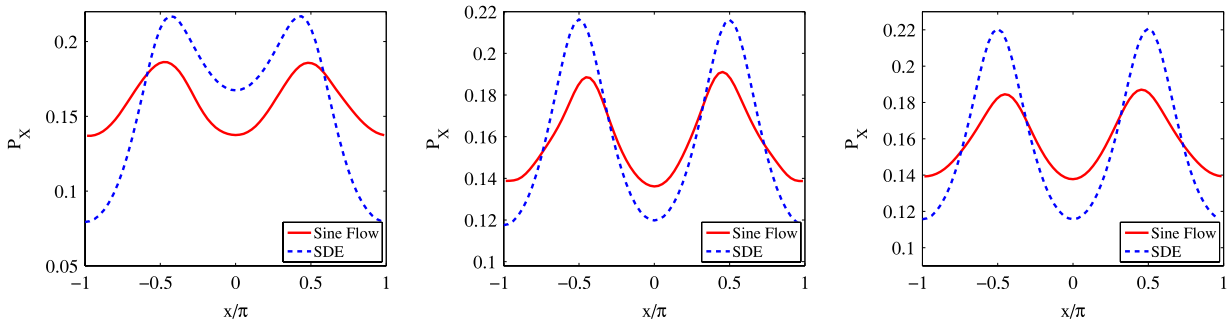

(a) $A_0 = 0.5$. (b) $A_0 = 1$. (c) $A_0 = 2$.

Fig. 7. PDF of the angle X as a function of flow amplitude A_0: comparison between the sine flow and the OU model. The comparison yields good qualitative agreement, despite the difference between the statistics of the underlying forcing terms in each model. Throughout this section $k = 2\pi/L = 1$.

in the second half-period. Integrating along the trajectory, we have

$$\frac{\mathrm{d}X}{1+\cos X} = -A_0 k \cos\left(ky_j + \phi_j\right) \mathrm{d}t,$$

$$X^{j+1/2} = 2\tan^{-1}\left[\tan\left(X^j/2\right) - A_0 k\,(\tau/2)\cos\left(ky_j + \phi_j\right)\right], \qquad (28)$$

in the first half-period, and

$$\frac{\mathrm{d}X}{1-\cos X} = A_0 k \cos\left(kx_{j+1} + \psi_j\right) \mathrm{d}t,$$

$$X^{j+1} = 2\cot^{-1}\left[\cot\left(X^{j+1/2}/2\right) - A_0 k\,(\tau/2)\cos\left(kx_{j+1} + \psi_j\right)\right] \qquad (29)$$

in the second. These results are substituted into the following formula for the Lagrangian tracer-gradient growth rate $\Lambda(\boldsymbol{x}_0)$. For a trajectory originating at $\boldsymbol{x}_0$, this is defined as

$$\Lambda(\boldsymbol{x}_0) := \lim_{T\to\infty} \frac{1}{T}\int_0^T -2\mu\left(\boldsymbol{x}\left(t';\boldsymbol{x}_0\right)\right)\sin X\left(\boldsymbol{x}\left(t';\boldsymbol{x}_0\right)\right)\,\mathrm{d}t'. \qquad (30)$$

For the sine flow, $\mu = d$ and X are piecewise constant on half-periodic intervals. The integral in Eq. (30) therefore converts into a sum. Splitting each period up into its first half and second half, the sum is

$$\Lambda(\boldsymbol{x}_0) = \lim_{N\to\infty} \frac{1}{N}\sum_{j=0}^{N}\left[-d^{j+1/2}\sin X^{j+1/2} - d^{j+1}\sin X^{j+1}\right], \qquad (31)$$

where $d^{j+1/2} = A_0 k\cos(ky_j + \phi_j)/2$ and $d^{j+1} = A_0 k\cos(kx_{j+1} + \psi_j)/2$ (Eq. (24)).

We examine the PDF of angles X generated by the sine flow and compare it with the PDF obtained from the model OU process. Our numerical results for the sine flow have been generated over 300,000 sine-flow periods with an ensemble of 75^2 particles. This ensures that the statistics have reached a steady state (the noisy phases are drawn from the uniform distribution on $[0, 2\pi)$). In this section, the sine-flow period is the standard unit of time, $\tau = 1$, and the box size $L = 2\pi$ is the standard unit of length. We nondimensionalise the OU model accordingly. The situation corresponds to a regime of rapid forcing because the correlation rate τ^{-1} is comparable to the typical strain and rotation rates, $A_0 k\tau = O(1)$. Thus, to mimic the stirring protocol (23) by an OU process, we identify the period τ of the sine flow with the OU decay timescales, $\tau_Y = \tau_Z = \tau = 1$, and we take $D_Y = D_Z = A_0^2 k^2/2$ Given the relations (24), we also take $w = c = 0$ in the OU model.

The resulting comparison (Fig. 7) shows qualitative similarities between the two systems: in both cases, the PDF of angles X is symmetric about $x = 0$, with maxima close to $x = \pm\pi/2$ (the sine-flow maxima deviate slightly from these values). When the maxima of the PDF coincide with $\pm\pi/2$, the tracer gradient aligns, on average, with the compressive direction. This qualitative similarity between the two PDFs is good, in view of the radically different noise-generating processes in each model: in the OU case, the noise terms are unbounded, while in the sine-flow case the fluctuations in Y and Z are bounded, $|Y|, |Z| \leq A_0 k$. We also compute the PDFs associated with the growth rate of the tracer gradient (Fig. 8). These are skewed towards positive values: on average, the tracer gradient grows exponentially. Finally, we examine the Eulerian structure of the flow by plotting the growth rate $\Lambda(\boldsymbol{x}_0)$ (Fig. 9). This is spatially homogeneous, thus underscoring the efficient nature of the random-phase sine flow in mixing the passive tracer. It also provides further justification for our application of the OU model to the problem in hand, since the flow statistics are, on average, the same along all trajectories.

5. Forced two-dimensional turbulence

In this section we compare the OU model of the orientation dynamics with the results of numerical simulations of two-dimensional turbulence. Unlike previous work [13], we focus on forced turbulence, which introduces rapid variations into the problem, and takes us into a parameter regime similar to the previous section (Section 4). Thus, we present results for the solution of the vorticity equation

$$\frac{\partial\omega}{\partial t} + \boldsymbol{u}\cdot\nabla\omega = -(-1)^p \nu_p \nabla^{2p}\omega + Q - \nu_0\omega, \qquad (32)$$

where Q is the forcing term and $-\nu_0\omega$ is a damping term that prevents a build-up of energy at large scales. (Simulations for Rayleigh damping [31] have also been carried out, and yield similar results.) To obtain a stochastic driving force on a particular scale k_e, we use the method developed by Lilly [32] (see also [25]). In this section, the space–time average $\langle\|Q\|_2^2\rangle^{-1/2}$ is the standard unit of time and the box size $L = 2\pi$ is the standard unit of length. The combination of damping and forcing in Eq. (32) yields a statistically steady state. Moreover, the tracer, driven by the flow (32), also reaches a steady state, in the sense that $\theta/\|\theta\|_2$ exhibits the so-called strange eigenmode [3,33]. Thus, it is legitimate to regard the late-time statistics of the angle β as being drawn from a stationary distribution. We solve Eq. (32) using a standard, semi-implicit pseudospectral method. We take the order of the viscosity to be $p = 8$; we also take $\nu_p = 10^{-35}$ in both the ω- and the θ-equations, and $\nu_0 = 0.05$. The spatial resolution is $N^2 = 512^2$ and the timestep is set to $\Delta t = 10^{-3}$; we have verified that the results are independent of gridsize and timestep with a convergence study.

We focus on evaluating the model parameters to maximise the overlap between the model and the DNS. To do this, we consider the Eulerian variables

$$\tilde{w} = \frac{1}{2}\omega + \partial_t\varphi + \boldsymbol{u}\cdot\nabla\varphi, \qquad \tilde{\mu} = \mathrm{sign}(d)\sqrt{d^2+s^2}.$$

In their book, Tennekes and Lumley [34] demonstrate the equivalence of Eulerian and Lagrangian averages in an incompressible

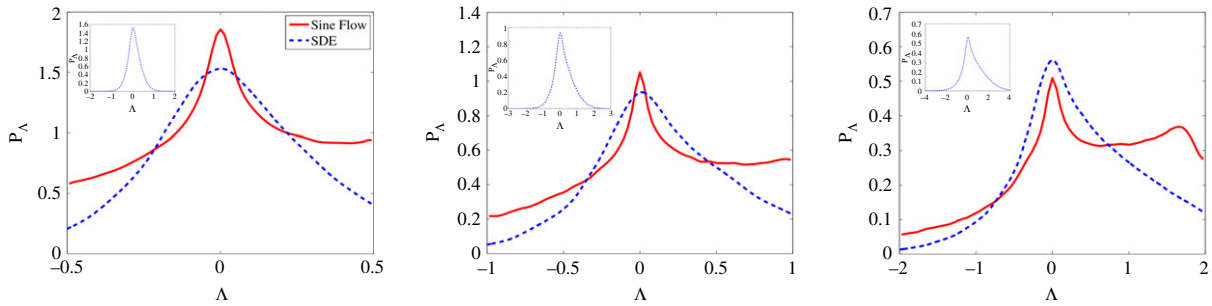

(a) $A_0 = 0.5$. (b) $A_0 = 1$. (c) $A_0 = 2$.

Fig. 8. PDF of the growth rate Λ as a function of flow amplitude A_0. In the main figures, we show a comparison between the OU model and the sine flow, while the insets contain the PDF of the OU model over an extended range. In the sine-flow case, the PDF takes values in a bounded interval, while the tails of the OU model extend to $\pm\infty$.

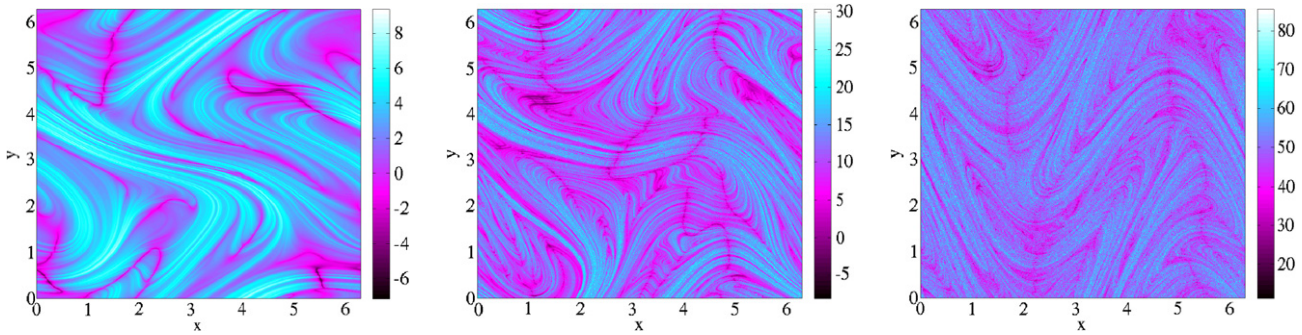

(a) $A_0 = 0.5$. (b) $A_0 = 1$. (c) $A_0 = 2$.

Fig. 9. The Lagrangian growth rate of the tracer gradient, $\Lambda(\boldsymbol{x}_0)$, according to Eq. (31).

fluid: if $F(\boldsymbol{x}, t)$ is a function to be integrated over the domain volume Ω, then

$$\int_\Omega F(\boldsymbol{x}(t;\boldsymbol{a}), t)\,\mathrm{d}^2\boldsymbol{a} = \int_\Omega F(\boldsymbol{x}, t)\,\mathrm{d}^2\boldsymbol{x},$$

where $\boldsymbol{a}$ labels the initial position of a typical Lagrangian particle. They also prove the stronger statement that the PDFs of the Lagrangian and Eulerian velocity fields are equivalent in homogeneous turbulence in an incompressible fluid (these results hold only for single-point statistics, and the two-point statistics differ). Moreover, the convergence to a limiting mean value is more rapid in this Eulerian case [35]. In view of these facts, computation of DNS-based expectation values is superior when undertaken in an Eulerian framework. Finally, we note that it suffices to estimate the widths of the model marginal distributions: once these have been extracted from the Eulerian statistics, the timescales $\tau_{Y,Z}$ do not matter, because in statistical equilibrium, the PDF is invariant under changes in $\tau_{Y,Z}$, provided the ratios

$$\frac{D_{Y,Z}}{\tau_{Y,Z}} := \sigma_{Y,Z}^2$$

are kept fixed; here $\sigma_{Y,Z}$ gives the width of the Y- and Z-distributions. We estimate the model width σ_Y to be $\langle\tilde{\mu}^2\rangle^{1/2} = 0.23$. Although Fig. 10(b) hints at the bimodality of the statistics of $\tilde{\mu}$, our estimate ensures that the most likely $\tilde{\mu}$-values from the DNS occur on the support of the model PDF $P_Y(y) \propto \mathrm{e}^{-y^2/(2\sigma_Y^2)}$. In a similar manner, we find that the PDF of $\tilde{w}$ has a Gaussian core (variance $\sigma_Z = 0.51$) and exponential tails: therefore, in order for the most likely $\tilde{w}$ values of the DNS to occur on the support of the model PDF $P_Z(z)$, we estimate the OU width to be the same as that of the Gaussian core, and take $P_Z(z) \propto \mathrm{e}^{-z^2/(2\sigma_Z^2)}$.

We compare the PDF of the angle X and the growth rate Λ, as generated both by the model OU process, and the two-dimensional turbulence. The results are shown in Fig. 11. The angle PDFs for the turbulence and for the OU model are in very close agreement, with large maxima at exactly $X = \pm\pi/2$. The most likely orientation of the tracer gradient is therefore $X = \pm/2$, which, according to Eq. (8), implies that the tracer gradient aligns with the compressive direction, in a statistical sense. The close agreement between the model and the DNS suggests that our equations have captured the physics of the orientation dynamics. Moreover, the result suggests that a small level of diffusion is unimportant in determining the preferred direction of the tracer gradient. The PDFs of the growth rate both demonstrate an asymmetry around $\Lambda = 0$ and a preference for positive values. Nevertheless, some differences are visible. In particular, the PDF of the DNS attains its maximum at a nonzero Λ-value, while the PDF of the model attains its maximum at zero. This discrepancy comes from the bimodality of the $\tilde{\mu}$-statistics. In contrast, the $\tilde{\mu}$-statistics of the sine flow (Section 4) are unimodal, and the flow and the model PDFs are qualitatively similar near $\Lambda = 0$ in that case. Finally, and in spite of this difference, the mean growth rate of the model and the DNS are identical in the first significant figure: $\Lambda_{1,\mathrm{OU}} = 0.1$; $\Lambda_{1,\mathrm{TURB}} = 0.1$. Moreover, because our model demonstrates 'fat tails', for a suitable choice of parameters D_Y and D_Z, it is possible to provide an upper bound on the growth rate of the DNS.

Finally, it is necessary to clarify whether the DNS corresponds to rapid forcing. Thus, we have computed the Lagrangian integral scales

$$T_{L,\mu} := \int_0^T \frac{\langle\mu(t)\mu(t+t')\rangle}{\langle\mu(t)^2\rangle}\mathrm{d}t',$$

$$T_{L,w} := \int_0^T \frac{\langle w(t)w(t+t')\rangle}{\langle w(t)^2\rangle}\mathrm{d}t',$$

along a Lagrangian trajectory starting at (π, π) (here T is sufficiently large to guarantee convergence of the integrals to a definite limit). Both timescales are $O\left(10^{-1}\right)$ in the nondimensional units described at the start of the section. Since $\langle\mu^2\rangle$ is $O(1)$, the

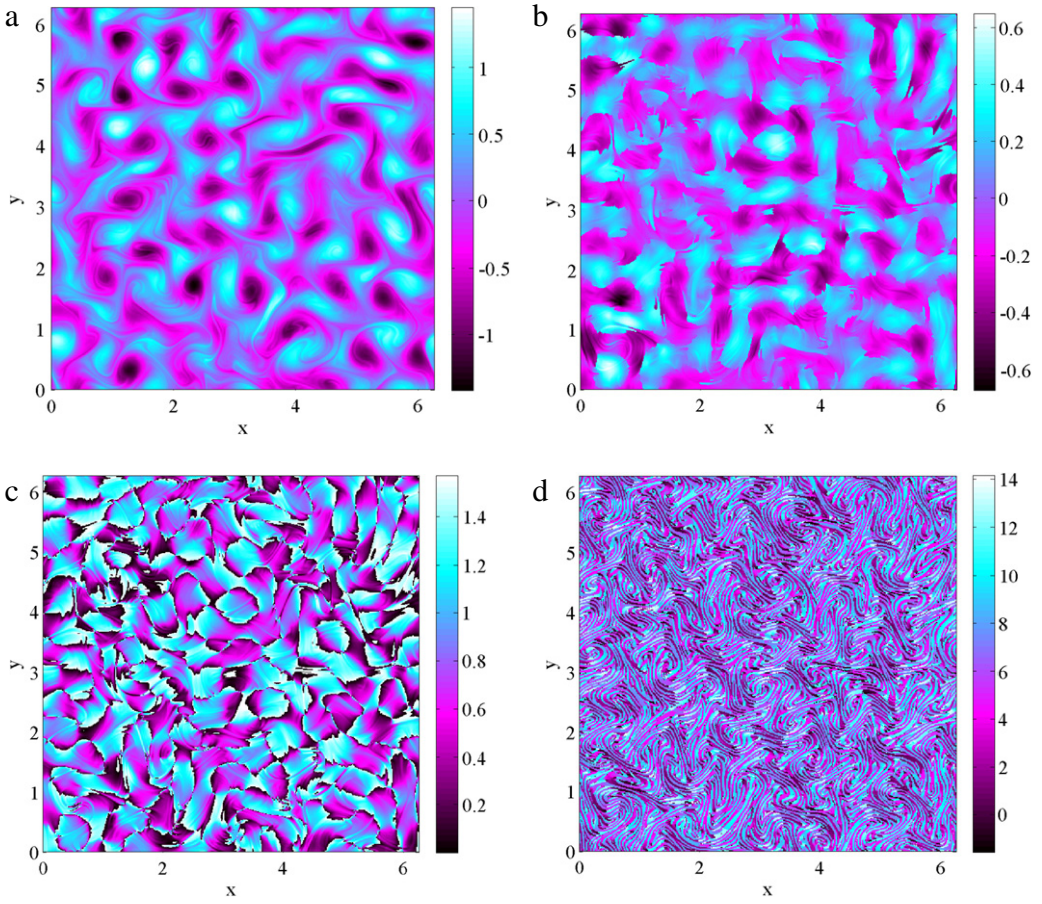

Fig. 10. Orientation dynamics of forced two-dimensional turbulence in a statistically steady state: snapshots of (a) the vorticity field ω; (b) the non-sign-definite eigenvalue $\tilde{\mu} = \text{sign}(d)\sqrt{s^2 + d^2}$; (c) the angle φ; (d) the angle X.

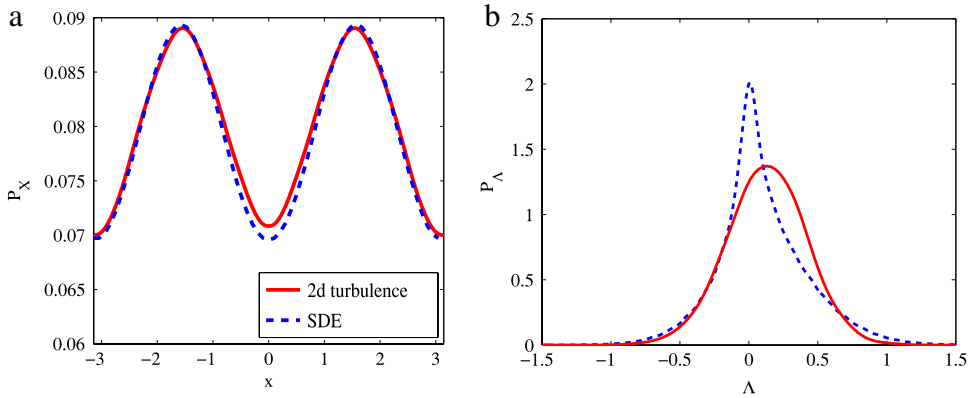

Fig. 11. (a) The PDF of the angle X according to the two-dimensional turbulence simulation (solid line), and the OU model (broken line). (b) The PDF of the growth rate. The model's description of the orientation statistics in (a) is in excellent agreement with the DNS; the agreement for the growth rate in (b) is less good. The latter comparison is spoiled by the difficulty in matching the model parameters to the DNS parameters, and by the fact that the distribution of strain $\tilde{\mu} = \text{sign}(d)\sqrt{d^2 + s^2}$ is in fact bimodal.

flow protocol studied in this section is rapid in the sense that the scale-free quantities $T_{L,\mu,w}\langle\mu^2\rangle^{1/2}$ are $O\left(10^{-1}\right)$, that is, the timescale defined by the typical value of strain is greater than or comparable to the timescales over which the strain and the effective rotation vary. These results confirm the usefulness of the OU description in modelling the growth rate of a tracer gradient under rapid stirring.

6. Conclusions

We have formulated a stochastic model of the orientation dynamics of a tracer gradient in a manner designed to mimic mixing under externally imposed temporally varying stirring in two dimensions. The model consists of a set of SDEs for the angle ζ, and for the forces that act thereon. The model is a general one that includes the adiabatic description of Lapeyre [13] as a special case. However, we focus mostly on the rapid case: we analyse the SDEs using the Fokker–Planck (FP) equation and compute the distribution of orientation angles and growth rates. The use of the FP equation yields some analytical results in the limit of zero correlation times: when the mean effective rotation is zero, the tracer gradient aligns, on average, with the compressive direction, and the mean growth rate of the tracer gradient is positive and given by an explicit expression in $\rho = D_Z/D_Y$ involving elliptic functions.

For finite correlation times and finite values of the effective rotation, numerical solutions suggest that the PDF is always skewed to positive values, producing a positive mean growth rate. We compare our model with two rapid-flow protocols: the random-phase sine flow, and forced two-dimensional turbulence. The qualitative agreement between the model PDFs and the PDFs generated from the flow protocols is good, and confirms the validity of the approach. Since our stochastic model is amenable both to mathematical and numerical analysis (the latter in minutes on a desktop computer), we anticipate its generalisation to three-dimensional flows.

Acknowledgements

The author wishes to thank M. Bustamante, D. D. Holm and J.-L. Thiffeault for helpful conversations.

References

[1] G. Falkovich, K. Gawędzki, M. Vergassola, Particles and fields in fluid turbulence, Rev. Modern Phys. 73 (2001) 913–975.
[2] R. Kraichnan, Convection of a passive scalar by a quasi-uniform random straining field, J. Fluid Mech. 64 (1974) 737–762.
[3] R.T. Pierrehumbert, Tracer microstructure in the large-eddy dominated regime, Chaos Solitons Fractals (1994) 1091–1110.
[4] A.A. Schekochihin, P.H. Haynes, S.C. Cowley, Diffusion of passive scalar in a finite-scale random flow, Phys. Rev. E 70 (2004) 046304.
[5] E. Balkovsky, A. Fouxon, Universal long-time properties of Lagrangian statistics in the Batchelor regime and their application to the passive-scalar problem, Phys. Rev. E 60 (1999) 4164–4174.
[6] D. Bernard, K. Gawędzki, Kupiainen, Slow modes in passive advection, J. Stat. Phys. 909 (1998) 519.
[7] G.K. Batchelor, The effect of homogeneous turbulence on material lines and surfaces, Proc. R. Soc. A 213 (1952) 349–366.
[8] S.B. Pope, P.K. Yeung, S.S. Girimaji, The curvature of material surfaces in isoptropic turbulence, Phys. Fluids A 8 (1989) 75–83.
[9] I.T. Drummond, W. Münch, Distortion of line and surface elements in model turbulent flows, J. Fluid Mech. 225 (1991) 529–543.
[10] M. Liu, F.J. Muzzio, The curvature of material lines in chaotic cavity flows, Phys. Fluids 1 (1996) 2010–2018.
[11] J.-L. Thiffeault, Stretching and curvature of material lines in chaotic flows, Physica D 198 (2004) 169–181.
[12] J.-L. Thiffeault, A.H. Boozer, The onset of dissipation in the kinematic dynamo, Phys. Plasmas 10 (2003) 259–265.
[13] G. Lapeyre, P. Klein, B.L. Hua, Does the tracer gradient vector align with the strain eigenvectors in 2D turbulence? Phys. Fluids 11 (1999) 3729–3737.
[14] J. Weiss, The dynamics of enstrophy transfer in two-dimensional hydrodynamics, Physica D 48 (1991) 273.
[15] G. Lapeyre, Characterization of finite-time Lyapunov exponents and vectors in two-dimensional turbulence, Chaos 12 (2002) 688–698.
[16] M. Gonzalez, P. Paranthoën, On the role of unsteady forcing of tracer gradient in local stirring, Eur. J. Mech. B 29 (2010) 143–152.
[17] A. Garcia, M. Gonzalez, P. Paranthoën, On the alignment dynamics of a passive scalar gradient in a two-dimensional flow, Phys. Fluids 17 (2005) 117102.
[18] M. Gonzalez, Kinematic properties of passive scalar gradient predicted by a stochastic Lagrangian model, Phys. Fluids 21 (2009) 055104.
[19] F. D'Ovidio, E. Shuckburgh, B. Legras, Local mixing events in the upper troposphere and lower stratosphere. Part I: detection with the Lyapunov diffusivity, J. Atmospheric Sci. 66 (2009) 3678–3694.
[20] K.S. Turitsyn, Polymer dynamics in chaotic flows with a strong shear component, J. Exp. Theor. Phys. 105 (2007) 655–664.
[21] H. Risken, The Fokker–Planck Equation, second ed., Springer, 1989.
[22] E. Dresselhaus, M. Tabor, The kinematics of stretching and alignment of material elements in general flow fields, J. Fluid Mech. 236 (1992) 415–444.
[23] J.D. Gibbon, D.D. Holm, The dynamics of the gradient of potential vorticity, J. Phys. A: Math. Theor. 43 (2010) 172001.
[24] P. Constantin, I. Procaccia, D. Segel, Creation and dynamics of vortex tubes in three-dimensional turbulence, Phys. Rev. E 51 (1995) 32073222.
[25] D. Molenaar, H.J.H. Clercx, G.J.F. van Heijst, Angular momentum of forced 2D turbulence in a square no-slip domain, Physica D (2004) 329–340.
[26] J.H. Li, Z.Q. Huang, Transport of particles caused by correlation between additive and multiplicative noise, Phys. Rev. E 57 (1998) 3917–3922.
[27] A. Barone, G. Paternò, Physics and Applications of the Josephson Effect, Wiley, 1982.
[28] V.V. Konotop, L. Vázquez, Nonlinear Random Waves, World Scientific Publishing, 1994.
[29] T.M. Antonsen Jr., Z. Fan, E. Ott, E. Garcia-Lopez, The role of chaotic orbits in the determination of power spectra, Phys. Fluids 8 (1996) 3094–3104.
[30] L. Ó Náraigh, J.-L. Thiffeault, Bubbles and filaments: stirring a Cahn–Hilliard fluid, Phys. Rev. E 75 (2007) 016216.
[31] T. DelSole, B.F. Farrell, A stochastically excited linear system as a model for quasigeostrophic turbulence: analytic results for one- and two-layer fluids, J. Atmospheric Sci. 52 (1995) 2531–2547.
[32] D.K. Lilly, Numerical simulation of two-dimensional turbulence, Phys. Fluids II (1969) 240–249.
[33] W. Liu, G. Haller, Strange eigenmodes and decay of variance in the mixing of diffusive tracers, Physica D (2003) 1–39.
[34] H. Tennekes, J.L. Lumley, A First Course in Turbulence, MIT Press, 1972.
[35] C. Pasquero, A. Provenzale, J.B. Weiss, Vortex statistics from Eulerian and Lagrangian time series, Phys. Rev. Lett. 89 (2002) 284501.